


# The topography of alpha-band activity tracks the content of spatial working memory

 **Joshua J. Foster**<sup>1,2,4</sup> **David W. Sutterer**<sup>1,2,4</sup> **John T. Serences**<sup>5,6</sup> **Edward K. Vogel**<sup>1,2,3,4</sup>  
and **Edward Awh**<sup>1,2,3,4</sup>

<sup>1</sup>Department of Psychology, The University of Chicago, Chicago, Illinois; <sup>2</sup>Institute for Mind and Biology, The University of Chicago, Chicago, Illinois; <sup>3</sup>Grossman Institute for Neuroscience, The University of Chicago, Chicago, Illinois; <sup>4</sup>Department of Psychology, University of Oregon, Eugene, Oregon; <sup>5</sup>Department of Psychology, University of California, San Diego, La Jolla, California; and <sup>6</sup>Neuroscience Graduate Program, University of California, San Diego, La Jolla, California

Submitted 8 September 2015; accepted in final form 13 October 2015

**Foster JJ, Sutterer DW, Serences JT, Vogel EK, Awh E.** The topography of alpha-band activity tracks the content of spatial working memory. *J Neurophysiol* 115: 168–177, 2016. First published October 14, 2015; doi:10.1152/jn.00860.2015.—Working memory (WM) is a system for the online storage of information. An emerging view is that neuronal oscillations coordinate the cellular assemblies that code the content of WM. In line with this view, previous work has demonstrated that oscillatory activity in the alpha band (8–12 Hz) plays a role in WM maintenance, but the exact contributions of this activity have remained unclear. Here, we used an inverted spatial encoding model in combination with electroencephalography (EEG) to test whether the topographic distribution of alpha-band activity tracks spatial representations held in WM. Participants in three experiments performed spatial WM tasks that required them to remember the precise angular location of a sample stimulus for 1,000–1,750 ms. Across all three experiments, we found that the topographic distribution of alpha-band activity tracked the specific location that was held in WM. Evoked (i.e., activity phase-locked to stimulus onset) and total (i.e., activity regardless of phase) power across a range of low-frequency bands transiently tracked the location of the sample stimulus following stimulus onset. However, only total power in the alpha band tracked the content of spatial WM throughout the memory delay period, which enabled reconstruction of location-selective channel tuning functions (CTFs). These findings demonstrate that alpha-band activity is directly related to the coding of spatial representations held in WM and provide a promising method for tracking the content of this online memory system.

working memory; alpha; EEG; oscillations; inverted encoding model

A RANGE OF EVIDENCE SUGGESTS that neuronal oscillations in the alpha band (8–12 Hz) play a central role in the selection and storage of information in the brain (Canolty and Knight 2010; Fries 2005; Klimesch 2012). For instance, many studies have shown that alpha-band activity covaries with the deployment of spatial attention, such that posterior alpha power is reduced contralateral to attended locations (e.g., Gould et al. 2011; Kelly et al. 2006; Thut et al. 2006). Indeed, the topographic distribution of alpha power not only tracks the attended visual hemifield, but also the specific retinotopic coordinates that are attended (Rihs et al. 2007; Worden et al. 2000). For example, Rihs and colleagues cued participants to attend to one of eight placeholder locations around a central fixation point and found that the topography of alpha power systematically varied with

the cued location, with more similar topographies associated with adjacent locations (Rihs et al. 2007). Extending these findings, others have decoded both horizontal and vertical shifts of attention from patterns of alpha power (Bahramisharif et al. 2010; van Gerven and Jensen 2009) and shown that lateralized modulations of alpha power are sensitive to the eccentricity of the attended location (Bahramisharif et al. 2011). Thus alpha-band activity enables tracking of the locus of spatial selective attention.

Here, motivated by past work positing a strong functional overlap between spatial attention and spatial working memory (WM) (Awh and Jonides 2001; Awh et al. 2006; Gazzaley and Nobre 2012), we examined whether alpha-band activity tracks spatial representations held in WM. Consistent with this possibility, past work has already shown that alpha power is reduced contralateral to locations held in spatial WM (Medendorp et al. 2007; Van Der Werf et al. 2008; van Dijk et al. 2010). However, these contralateral modulations do not establish whether alpha-band activity, as in the case of spatial selective attention, tracks the specific locations that are stored. Instead, these modulations might reflect a lateralized memory operation (e.g., a top-down control signal) that tracks the visual hemifield of the remembered location but not the exact location that is stored. Here, we tested whether alpha-band activity relates to the coding of the precise positions stored in WM, rather than a lateralized memory process that is not sensitive to the specific content of spatial WM.

In three experiments, participants performed spatial WM tasks that required them to remember the precise angular location of a stimulus, sampled from a 360° space. Using an inverted spatial encoding model (IEM) (Brouwer and Heeger 2009, 2011; for review, see Sprague et al. 2015), we identified the oscillatory frequency bands in which the topographic distribution of power, measured using EEG, carried location-specific information. We found that the topographic distribution of both evoked (i.e., activity phase-locked to stimulus onset) and total (i.e., activity regardless of phase) power across a range of low-frequency bands transiently tracked stimulus location. However, only the topography of total power in the alpha band tracked the content of spatial WM throughout the delay period, indicating that alpha-band activity is directly related to the coding of spatial representations held in WM. The IEM allowed us to reconstruct spatially specific response profiles (termed channel tuning functions, or CTFs) that tracked the stored location during both encoding and delay

Address for reprint requests and other correspondence: J. J. Foster, Institute for Mind and Biology, The Univ. of Chicago, 940 East 57th St., Chicago, IL 60637 (e-mail: joshuafofoster@uchicago.edu).

periods of WM tasks. Thus alpha-band activity enables time-resolved tracking of spatial representations held in WM. These findings underscore the central role that alpha-band activity plays in coding the content of spatial WM and provide new evidence for the functional overlap between spatial WM and spatial attention.

## MATERIALS AND METHODS

### Participants

Fifteen volunteers took part in each experiment for monetary compensation (\$10/h). The participants in each experiment were nonoverlapping, with the exception of one participant who took part in both *experiments 1* and *3*. Participants reported normal or corrected-to-normal vision, were between 18 and 35 yr old, and provided informed consent according to procedures approved by the University of Oregon Institutional Review Board. Participants were replaced if more than 25% of trials were lost due to recording or ocular artifacts, and/or if the participants did not complete all trials during the session (5 in *experiment 1*, 7 in *experiment 2*, and 3 in *experiment 3*).

### Stimulus Displays

Stimuli were generated in Matlab (Mathworks) using the Psychophysics Toolbox (Brainard 1997; Pelli 1997) and were presented on a 17-in. CRT monitor (refresh rate: 60 Hz) at a viewing distance of ~100 cm. All stimuli were rendered in dark gray against a medium gray background.

The spatial WM tasks required participants to remember the angular location of a sample stimulus. The stimulus was a circle (1.6° in diameter) centered 4° of visual angle from the central fixation point (0.2° in diameter). For each trial, the angular location of the stimulus was sampled from one of eight location bins spanning 0–315° (in angular location), in steps of 45°, with jitter added to cover all 360° of possible locations to prevent categorical coding of stimulus location. In all experiments, the location of the sample stimulus was drawn from each bin equally often, and in a random order, within each block of trials.

### Procedures

After providing informed consent, participants were fitted with a cap embedded with 20 scalp electrodes before completing a spatial WM task (see below for details). Testing took place in a dimly lit, electrically shielded chamber. In each experiment, the spatial WM task comprised 15 blocks of 64 trials, and took approximately 2–2.5 h to complete.

**Delayed estimation task.** Participants in *experiments 1* and *2* performed a spatial delayed-estimation task (Wilken and Ma 2004; Zhang and Luck 2008; see Fig. 1A). These experiments differed only in trial timing. Participants began each trial by pressing the spacebar. The trial began with a fixation display lasting between 600 and 1,500 ms. A sample stimulus was then presented (250 ms in *experiment 1*; 1,000 ms in *experiment 2*), followed by a delay period during which only the fixation point remained visible (1,750 ms in *experiment 1*; 1,000 ms in *experiment 2*). After the delay period, participants used a mouse to click on the perimeter of a probe ring (8° in diameter, 0.2° thick) to report the remembered location of the sample stimulus as precisely as possible. Before starting the task, participants completed a brief set of practice trials to ensure they understood the task.

**Spatial change detection task.** Participants in *experiment 3* performed a spatial change detection task (see Fig. 1B). Rather than reporting the remembered location after the delay period with a mouse click, a test stimulus (identical to the sample stimulus) was presented for 250 ms. On half of trials, the test stimulus was presented in the same location as the sample stimulus (no-change trials), while on the

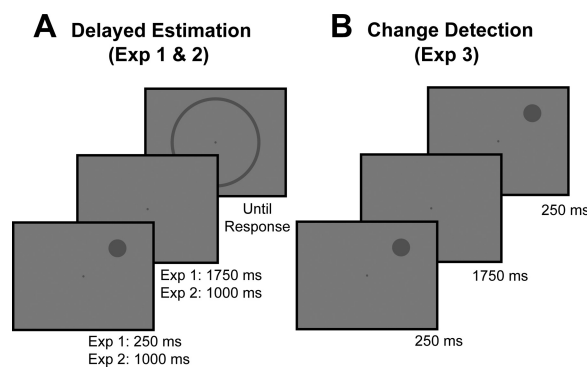


Fig. 1. Spatial working memory (WM) tasks. *A*: in *experiments 1* and *2*, participants performed a delayed estimation task. Participants maintained fixation while they remembered the angular location of a sample stimulus, which they reported after a delay period by clicking on the perimeter of a rim. *Experiments 1* and *2* differed only in trial timing. *B*: in *experiment 3*, participants performed a change detection task. Rather than report the location of the sample stimulus, a test stimulus was presented after the delay period and participants reported whether or not the location of the stimulus had changed. Stimuli not perfectly to scale.

other half of trials the test stimulus was shifted 20° clockwise or anticlockwise from the sample location (change trials). Participants indicated with a key press whether or not the location of the stimulus had changed. The timing of the task was identical to *experiment 1* (i.e., 250-ms sample stimulus, 1,750-ms delay period). Before starting the task, participants completed a brief set of practice trials with feedback to ensure they knew the size of the change to expect for change trials.

### Modeling Response Error Distributions

In the delayed estimation experiments (*experiments 1* and *2*), response error, the angular difference between the reported and presented locations, could range from  $-180^\circ$  to  $180^\circ$ . The response error distribution for each participant was modeled as the mixture of a von Mises distribution and a uniform distribution, corresponding to trials in which the sample stimulus was successfully or unsuccessfully stored, respectively (see Zhang and Luck 2008). Maximum likelihood estimates were obtained for three parameters: 1) the mean of the von Mises component ( $\mu$ ), corresponding to response bias; 2) the dispersion of the von Mises distribution (*s.d.*), corresponding to mnemonic precision; and 3) the height of the uniform distribution ( $P_f$ ), corresponding to the probability of forgetting the sample stimulus. Parameter estimates were obtained using the “MemFit.m” function of MemToolbox (Suchow et al. 2013).

### EEG Acquisition

We recorded EEG from 20 tin electrodes mounted in an elastic cap (Electro-Cap International, Eaton, OH). We recorded from International 10/20 sites F3, FZ, F4, T3, C3, CZ, C4, T4, P3, PZ, P4, T5, T6, O1, and O2, along with five nonstandard sites: OL midway between T5 and O1, OR midway between T6 and O2, PO3 midway between P3 and OL, PO4 midway between P4 and OR, and POz midway between PO3 and PO4. All sites were recorded with a left-mastoid reference, and were re-referenced offline to the algebraic average of the left and right mastoids. To detect horizontal eye movements, horizontal electrooculogram (EOG) was recorded from electrodes placed ~1 cm from the external canthus of each eye. To detect blinks and vertical eye movements, vertical EOG was recorded from an electrode placed below the right eye and referenced to the left mastoid. The EEG and EOG were amplified with an SA Instrumentation amplifier with a bandpass of 0.01–80 Hz and were digitized at 250 Hz using LabVIEW 6.1 running on a PC. Trials were visually

inspected for artifacts, and we discarded trials contaminated by blocking, blinks, detectable eye movements, excessive muscle noise, or skin potentials. An average of 12.3% (SD = 5.5%) of trials were rejected per participant across all three experiments.

### Time-Frequency Analysis

Time-frequency analyses were performed using Matlab in conjunction with the Signal Processing toolbox and the EEGLAB toolbox (Delorme and Makeig 2004). To isolate frequency-specific activity, the raw EEG signal was bandpass filtered using a two-way least-squares finite impulse response filter (“eegfilt.m” from EEGLAB Toolbox; see Delorme and Makeig 2004). This filtering method uses a zero-phase forward and reverse operation, which ensures that phase values are not distorted, as can occur with forward-only filtering methods. A Hilbert Transform (Matlab Signal Processing Toolbox) was applied to the bandpass-filtered data, producing the complex analytic signal,  $z(t)$ , of the filtered EEG,  $f(t)$ , where  $z(t) = f(t) + i\tilde{f}(t) = A(t)e^{i\phi(t)}$ , from which instantaneous amplitude,  $A(t)$ , was extracted;  $\tilde{f}(t)$  is the Hilbert Transform of  $f(t)$ , and  $i = \sqrt{-1}$ . The complex analytic signal was extracted for each electrode using the following Matlab syntax:

```
hilbert(eegfilt(data, F, f1, f2)')
```

where data is a 2D matrix of raw EEG (number of trials  $\times$  number of samples),  $F$  is the sampling frequency (250 Hz),  $f1$  is the lower bound of the filtered frequency band, and  $f2$  is the upper bound of the filtered frequency band. For alpha-band analyses, we used an 8- to 12-Hz bandpass filter; thus  $f1$  and  $f2$  were 8 and 12, respectively. For the time-frequency analysis, we searched a broad range of frequencies (4–50 Hz, in increments of 1 Hz with a 1-Hz bandpass). For these analyses  $f1$  and  $f2$  were 4 and 5 to isolate 4- to 5-Hz activity; 5 and 6 to isolate 5- to 6-Hz activity; and so on.

Total power was computed by squaring the complex magnitude of the complex analytic signal, and then averaging across trials. Thus total power reflects ongoing activity irrespective of its phase relationship to onset of the sample stimulus. In contrast, evoked power was calculated by first averaging the complex analytic signal across trials, and then squaring the complex magnitude of the averaged analytic signal. Evoked power reflects activity phase-locked to stimulus onset because only activity with consistent phase across trials remains after averaging the complex analytic signal.

Because calculating evoked power requires averaging across trials, artifact-free trials were partitioned into three blocks. To prevent bias in our analysis, we equated the number of observations across location bins within each block. To this end, we calculated the minimum number of trials for any given location bin  $n$  for each participant, and assigned  $n/3$  many trials for each location bin to each of the three blocks. Importantly, the blocks were independent (i.e., no trial was repeated across blocks) to prevent circularity in the cross-validation procedures used for the IEM routine (see *Inverted Encoding Model*). Evoked and total power were then calculated for each location bin for each block, resulting in an  $l*b \times m \times s$  matrix of both evoked and total power values, where  $l$  is the number of location bins,  $b$  is the number of blocks,  $m$  is the number of electrodes, and  $s$  is the number of time samples. For the analysis in which the IEM is applied across many frequency bands, we downsampled the data matrix to a sample rate of 50 Hz (i.e., one sample every 20 ms) to reduce computation time. The data matrix was not downsampled for analyses restricted to the alpha band.

Finally, because we equated the number of trials across location bins within blocks, a random subset of trials were not included in any block. Thus we randomly generated multiple block assignments (five for the full time-frequency analyses, and ten for the alpha-band analyses), each resulting in an  $l*b \times m \times s$  power matrix. The IEM routine (see *Inverted Encoding Model*) was applied to the matrices of

power values for each block assignment, and their outputs (i.e., channel response profiles) were averaged. This approach better utilized the complete data set for each participant and minimized the influence of idiosyncrasies in estimates of evoked and total power specific to certain assignments of trials to blocks.

### Inverted Encoding Model

We used an IEM to reconstruct location-selective CTFs from the topographic distribution of oscillatory power across electrodes. We assumed that power measured at each electrode reflects the weighted sum of eight spatial channels (i.e., neuronal populations), each tuned for a different angular location (cf. Brouwer and Heeger 2009, 2011; Sprague and Serences 2013; Sprague et al. 2014). We modeled the response profile of each spatial channel across angular locations as a half sinusoid raised to the seventh power, given by:

$$R = \sin(0.5\theta)^7$$

where  $\theta$  is angular location (ranging from  $0^\circ$  to  $359^\circ$ ), and  $R$  is the response of the spatial channel in arbitrary units. This response profile was circularly shifted for each channel such that the peak response of each spatial channel was centered over one of the eight location bins (i.e.,  $0^\circ$ ,  $45^\circ$ ,  $90^\circ$ , etc.). The predicted channel responses for each location bin were derived from these basis functions (calculated using the angular location at the center of each bin).

An IEM routine was applied to each time-frequency point in the time-frequency analyses, and to each time point in the alpha-band analyses. This routine proceeded in two stages (train and test). In the training stage, training data  $B_1$  were used to estimate weights that approximate the relative contribution of the eight spatial channels to the observed response measured at each electrode. Let  $B_1$  ( $m$  electrodes  $\times n_1$  observations) be the power at each electrode for each measurement in the training set,  $C_1$  ( $k$  channels  $\times n_1$  observations) be the predicted response of each spatial channel (determined by the basis functions) for each measurement, and  $W$  ( $m$  electrodes  $\times k$  channels) be a weight matrix that characterizes a linear mapping from “channel space” to “electrode space”. The relationship between  $B_1$ ,  $C_1$ , and  $W$  can be described by a general linear model of the form:

$$B_1 = WC_1$$

The weight matrix was obtained via least-squares estimation as follows:

$$\hat{W} = B_1 C_1^T (C_1 C_1^T)^{-1}$$

In the test stage, with the weights in hand, we inverted the model to transform the observed test data  $B_2$  ( $m$  electrodes  $\times n_2$  observations) into estimated channel responses,  $\hat{C}_2$  ( $k$  channels  $\times n_2$  observations):

$$\hat{C}_2 = (\hat{W}^T \hat{W})^{-1} \hat{W}^T B_2$$

Each estimated channel response function was circularly shifted to a common center (i.e.,  $0^\circ$  on the “Channel Offset” axes of the figures) by aligning the estimated channel responses to the channel tuned for the stimulus bin to yield CTFs. The IEM routine was performed separately for each sample point from 500 ms prior to stimulus onset through to the end of the delay period (2000 ms).

Importantly, we used a “leave-one-out” cross validation routine such that two blocks of estimated power values (see *Time-Frequency Analysis*) served as  $B_1$  and were used to estimate  $W$ , and the remaining block served as  $B_2$  and was used to estimate  $C_2$ . Thus the training and test data were always independent. This process was repeated until each of the three blocks were held out as the test set, and the resulting CTFs were averaged across each test block.

Finally, because the exact contributions of each spatial channel to each electrode (i.e., the channel weights,  $W$ ) will likely vary by subject, the IEM routine is applied separately for each subject, and

statistical analyses were performed on the reconstructed CTFs. This approach allowed us to disregard differences in how location selectivity is mapped to scalp-distributed patterns of power across subjects, and instead focus on the profile of activity in the common stimulus or “information” space (Sprague and Serences 2015).

### Statistical Analysis

To quantify the location selectivity of CTFs, we used linear regression to estimate CTF slope (i.e., slope of channel response as a function of location channels after collapsing across channels that were equidistant from the channel tuned to the location of the evoking stimulus), where higher CTF slope indicates greater location selectivity. To test whether CTF selectivity was reliably above chance, we tested whether CTF slope was greater than zero using a one-sample *t*-test. Because mean CTF slope may not be normally distributed under the null hypothesis, we employed a Monte Carlo randomization procedure to empirically approximate the null distribution of the *t*-statistic. Specifically, we implemented the IEM as described above but randomized the location labels within each block so that the labels were random with respect to the observed responses in each electrode. This randomization procedure was repeated 1,000 times to obtain a null distribution of *t*-statistics. To test whether the observed CTF selectivity was reliably above chance, we calculated the probability of obtaining a *t*-statistic from the surrogate null distribution greater than or equal to the observed *t*-statistic (i.e., the probability of a Type 1 Error). Our permutation test was therefore a one-tailed test. CTF selectivity was deemed reliably above chance if the probability of a Type 1 Error was less than 0.01. This permutation testing procedure was applied to each time-frequency point in the time-frequency analyses, and to each time point in the alpha-band analyses.

### Quantifying Biases in Eye Position

Although we discarded trials with detectable eye movements, small but systematic biases in eye position toward the remembered location may still exist. Indeed, we found evidence for very small but reliable biases in horizontal EOG amplitude that tracked stimulus location (see RESULTS). If eye position is biased towards stimulus location, then there should be a linear relationship between the horizontal position of the stimulus and horizontal EOG amplitude. Thus we used linear regression to calculate an eye bias score to quantify the extent to which eye position covaried with stimulus location. The eye bias score was calculated as the slope of the best fitting linear function describing horizontal EOG amplitude (in  $\mu$ V) as a function of the horizontal location of the stimulus (in degrees of visual angle). Higher eye bias scores therefore reflect greater changes in eye position as a function of stimulus location. This eye bias score was calculated across time for each participant separately.

## RESULTS

### Behavior

Task performance confirmed that participants were engaged in the spatial WM tasks in all three experiments. In the delayed-estimation experiments (*experiment 1* and *2*), mnemonic precision computed from a mixture model (Suchow et al. 2013; Zhang and Luck 2008) was high, indicated by low *s.d.* values (*experiment 1*:  $M = 6.6^\circ$ ,  $SD = 1.8^\circ$ ; *experiment 2*:  $M = 5.2^\circ$ ,  $SD = 1.6^\circ$ ), and the probability that the stimulus was forgotten,  $P_f$ , was extremely low (*experiment 1*:  $M = 0.002$ ,  $SD = 0.002$ ; *experiment 2*:  $M = 0.002$ ,  $SD = 0.002$ ). In the spatial change detection task (*experiment 3*), change detection accuracy was high ( $M = 90.1\%$ ,  $SD = 4.7\%$ ).

### Experiment 1: Identifying Frequency Bands that Track the Content of Spatial Working Memory

We first sought to identify the frequency bands in which the topographic distribution of oscillatory power tracked the content of spatial WM. To this end, we used an IEM to reconstruct location-selective CTFs (see MATERIALS AND METHODS). Using the IEM, we searched a broad range of frequencies (4–50 Hz, in increments of 1 Hz) across time to identify the frequency bands in which the topographic distribution of evoked and total power tracked the location of the sample stimulus. If the multivariate pattern of power across electrodes carries information about stimulus location, then the IEM should reveal a graded CTF profile, with a clear peak in the channel tuned for the remembered location. On the other hand, if the multivariate pattern of power does not carry information about stimulus location, then the IEM should produce a flat CTF profile, indicating no location tuning. Figure 2 shows location selectivity of reconstructed CTFs (as measured by CTF slope) as a function of time and frequency for both evoked and total power. We performed a permutation test at each time-frequency point to identify the points at which CTF slope was reliably above zero (see MATERIALS AND METHODS). We found the topographic distribution of both evoked and total power transiently tracked the location of the sample stimulus across a range of low frequencies ( $\sim 4$ – $20$  Hz; Fig. 2A). In contrast, only total alpha power ( $\sim 8$ – $12$  Hz) enabled sustained tracking of the stored location throughout the blank delay (Fig. 2B). Thus the topographic distribution of total alpha power tracked spatial representations held in WM.

*Alpha power tracks the content of spatial WM with fine-grained spatial resolution.* Previous work has demonstrated that alpha power decreases contralateral to a location held in spatial WM (Medendorp et al. 2007; Van Der Werf et al. 2008;

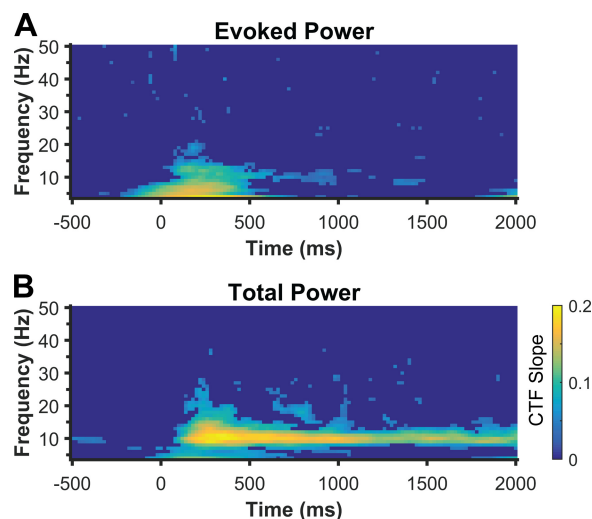


Fig. 2. Identifying the frequency bands that track the content of spatial WM in *experiment 1*. An IEM was used to reconstruct location-selective channel tuning functions (CTFs) from the topographic distribution of evoked (A) or total (B) power across a broad range of frequencies (4–50 Hz, in increments of 1 Hz) and time. Evoked and total power transiently tracked stimulus location after stimulus onset across a broad range of frequencies (4 to  $\sim 20$  Hz). However, only total alpha power tracked the content of spatial WM throughout the delay period. Color represents CTF slope, a measure of CTF selectivity that quantifies the location-specific activity in the topographic distribution of power. Points at which CTFs slope was not reliably above zero as determined by a permutation test are set to zero (dark blue).

van Dijk et al. 2010). It is possible that location selectivity in the alpha band, measured using CTF slope, simply reflects sensitivity of alpha power to the hemifield (or quadrant) of the remembered location. Such coarse location tuning could give rise to a graded CTF when shifted and averaged across location bins. To test this possibility, we examined the channel response profiles reconstructed from total alpha (8–12 Hz) power in *experiment 1* for each of the eight location bins separately. If the topographic distribution of alpha power tracks the precise location held in WM, then the channel response profiles should differ for each of the eight location bins. Specifically, for each location bin, we should observe a graded tuning profile, with a peak response in the channel tuned for the remembered location. Figure 3 shows the channel responses (averaged across time from 0 to 2,000 ms) for each of the eight location bins. Indeed, we found that the peak channel response was always seen in the channel tuned for the remembered location, providing clear evidence that the topography of alpha power tracked the specific angular location held in WM.

*Examining the format of spatial representations tracked by alpha power.* Next we examined the format of the spatial representations tracked by the topographic distribution of alpha power. Our standard basis set specified a “graded” channel response profile, with the peak response in the channel tuned for the remembered location, and with gradually diminishing response for channels tuned for other locations. This graded response profile across feature-selective cells is the hallmark of population coding of sensory variables (Pouget et al. 2000), rather than more abstracted (e.g., categorical) representations. We found that CTFs reconstructed from alpha-band activity showed this graded profile, suggesting that modulations of alpha power follow a graded, sensory format (Fig. 4A). However, using an IEM, it is always possible that the graded CTF profile reflects the graded basis function itself rather than truly graded location-selective activity (Ester et al. 2015; Saproo and Serences 2014). To rule out this possibility, we reconstructed CTFs with the IEM, this time with a modified basis set of eight orthogonal Kronecker delta functions, each centered on one of the eight location bins. These functions do not specify a graded profile of responses across channels. Thus, if a graded profile

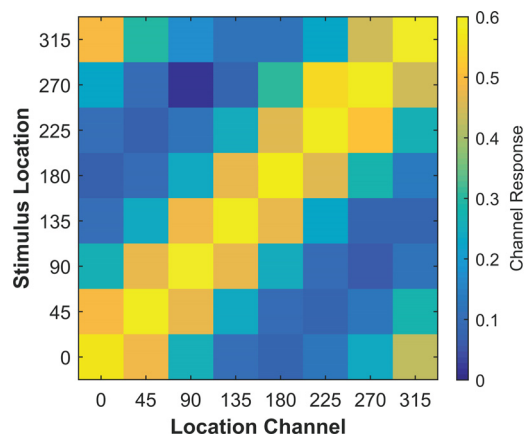


Fig. 3. Unshifted channel responses reconstructed from total alpha power after stimulus onset (averaged from 0–2,000 ms) shown for each of the eight stimulus location bins in *experiment 1*. For all location bins, the peak response is seen in the channel tuned for that stimulus location, confirming that the topography of alpha power tracked the precise location held in spatial WM.

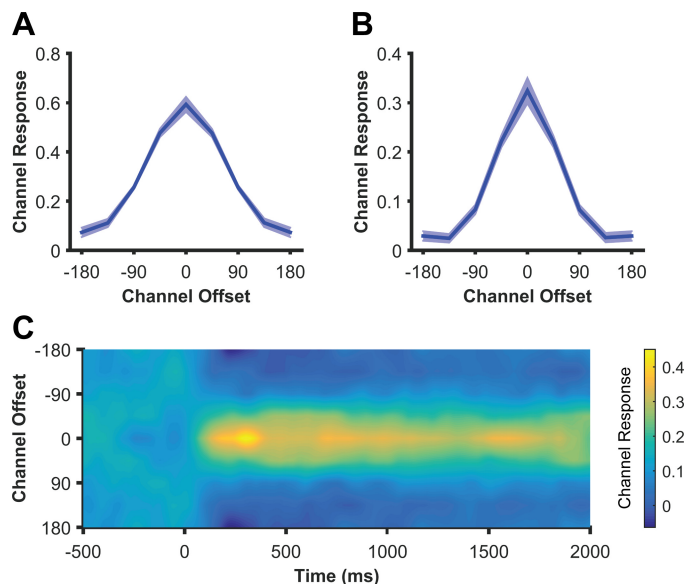


Fig. 4. CTFs reconstructed from total alpha (8–12 Hz) power after stimulus onset (averaged from 0–2,000 ms) using the standard, “graded” basis set (A) and using a basis set of eight orthogonal Kronecker delta functions (B) for *experiment 1*. CTFs reconstructed using the orthogonal basis set still showed a smooth, graded profile, demonstrating that the intrinsic tuning properties of alpha power are well-described by the graded basis function of the spatial encoding model. Shaded error bars reflect bootstrapped standard error of the mean. C: time-resolved CTF reconstructed using the orthogonal basis set, showing that the graded CTF profile was consistent across time points.

is observed using this basis function it must reflect a graded pattern in the data itself. In contrast, if the spatial representations tracked by alpha-band power do not follow this graded format, we would expect to recover a peak in the channel tuned for the remembered location, and uniform responses across the rest of the channels. Using this orthogonal basis set, reconstructed CTFs had a graded profile (Fig. 4B), confirming that graded location tuning is an intrinsic property of alpha activity and is not imposed by the graded basis function. Figure 4C shows that this graded profile was consistent across time. Therefore, alpha-band activity follows the expected format of a sensory code.

*Ruling out biases in eye position.* Eye movements generate electrical potentials that affect EEG recordings. We instructed participants to maintain fixation during the spatial WM task, and discarded trials with detectable eye movements. Nevertheless, small but systematic biases in eye position toward the remembered location may still exist. To examine this possibility, we inspected horizontal electrooculogram as a function of stimulus location. We found a reliable bias in eye position that tracked stimulus position. However, this bias was remarkably small ( $<2 \mu\text{V}$ ), corresponding to shifts from fixation of less than  $0.15^\circ$  of visual angle on average (Lins et al. 1993a, 1993b). We found that CTF slope in the alpha-band is greatest early in the trial, and decreased toward the end of the delay period (Fig. 5A). In contrast, bias in eye position, quantified using an eye bias metric (see MATERIALS AND METHODS), increased gradually as the delay period progressed (Fig. 5B). Therefore, subtle biases in eye position cannot explain the link between alpha activity and the content of spatial WM.

### Experiment 2: Alpha Activity Tracks Spatial Representations When the Stimulus Remains in View

In *experiment 1*, we demonstrated that topographic patterns of alpha power track the content of spatial WM during the delay period of a WM task. Recent work suggests that WM is important not only for maintaining representations of stimuli that are no longer externally available but also for representing stimuli that remain within view (Chun 2011; Tsubomi et al. 2013). In *experiment 2*, we used an extended encoding period (1,000 ms) to examine whether the topographic distribution of alpha power tracks the spatial representation of a stimulus that remains in view. We observed location-selective CTFs reconstructed from total alpha activity (Fig. 6B). Importantly, robust CTFs were seen throughout both the stimulus (0–1,000 ms) and delay (1,000–2,000 ms) periods, demonstrating that alpha activity tracks the location of a to-be-remembered stimulus, even when the stimulus remains in view. Thus total alpha power tracks spatial representations both in the presence and absence of visual input.

In *experiment 2*, we again found that evoked alpha power generated reliable CTFs following stimulus onset (Fig. 6A). However, weak but reliable CTF selectivity was also seen following stimulus offset (at 1,000 ms). This second burst of location-specific evoked activity may reflect resynchronization of low-frequency activity caused by the abrupt visual transient of stimulus offset (Gruber et al. 2005; Hanslmayr et al. 2007). However, further work is necessary to test this possibility.

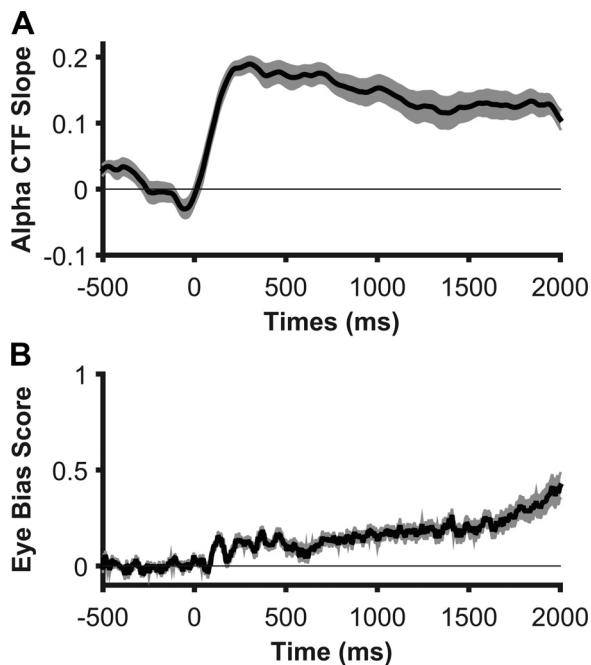


Fig. 5. Alpha CTF selectivity and small biases in eye position toward the remembered location show different time courses. *A*: location-selectivity of CTFs reconstructed from total alpha (8–12 Hz) power across time. Although CTF selectivity is robust throughout the delay period, it gradually declines across time. *B*: eye bias score quantifying bias in eye position toward (positive values) or away (negative values) from the remembered location. This score reflects the change in HEOG amplitude (in  $\mu\text{V}$ ) seen when the horizontal stimulus position changes by one degree of visual angle. In contrast to CTF selectivity, bias in eye position toward the remembered location increases across time, demonstrating that location-selective patterns of alpha power are not accounted for by small but reliable biases in eye position. Shaded error bars reflect bootstrapped standard error of the mean.

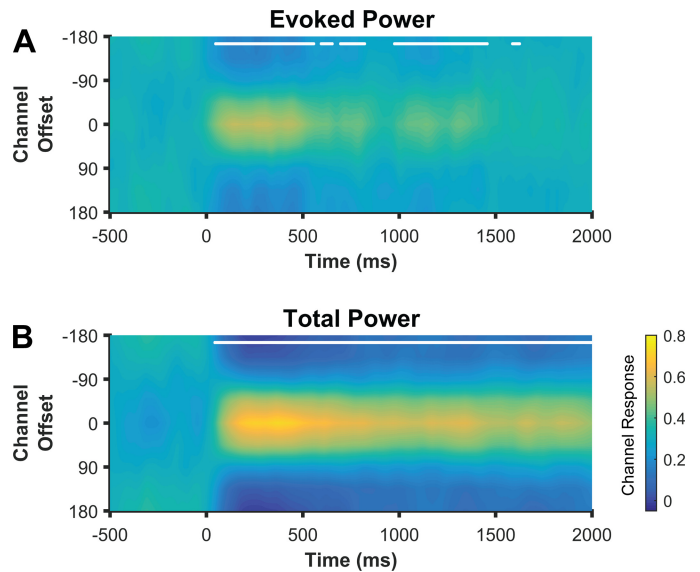


Fig. 6. Total alpha activity tracks stimulus location when the stimulus remains in view. Location CTFs reconstructed from evoked (*A*) and total (*B*) alpha (8–12 Hz) activity during the spatial WM task with a long encoding period (1,000 ms; *experiment 2*). Despite the stimulus remaining in view from 0 to 1,000 ms, total alpha power tracked stimulus location during this period, demonstrating that total alpha power tracks spatial representations both in the presence and absence of visual input. Evoked alpha power showed reliable but weaker location selectivity during the delay period. White markers along the top of the panels indicate the points at which CTF slope was reliably above chance as determined by a permutation test.

### Experiment 3: Ruling Out Response Confounds

In our first two experiments, we used a delayed-estimation task in which participants used a mouse to click on a ring around fixation to report the remembered location (Fig. 1A). Consequently, the remembered location covaried with the required response. In *experiment 3*, we sought to rule out the possible contribution of preparatory motor activity to the location-selective CTFs that we observed in the delayed-estimation task. To this end, participants performed a spatial change detection task, in which they remembered the precise location of a sample stimulus, and reported whether the location of a test stimulus, presented after the delay period, differed from that of the sample stimulus (Fig. 1B). Critically, participants could not plan their response (“change” vs. “no change”) until the test stimulus was presented. Therefore, any location-selective delay activity cannot reflect a planned response. As in *experiment 1*, evoked CTFs only transiently tracked stimulus location (Fig. 7A), while the topographic distribution of total alpha power tracked the remembered location, allowing for the reconstruction of reliable CTFs throughout the delay period (Fig. 7B). Thus findings from *experiment 3* solidify our conclusion that alpha activity tracks the contents of spatial memory, rather than the trajectory of a planned response.

### Location-Selective Activity Is Specific to the Alpha-Band: A Cross-Experiment Analysis

In our analyses of *experiments 2* and *3* so far, we focused exclusively on the alpha band (8–12 Hz) because this frequency band was implicated in WM storage in *experiment 1*. These analyses replicated the finding that the topographic distribution of alpha power tracks the content of spatial WM.

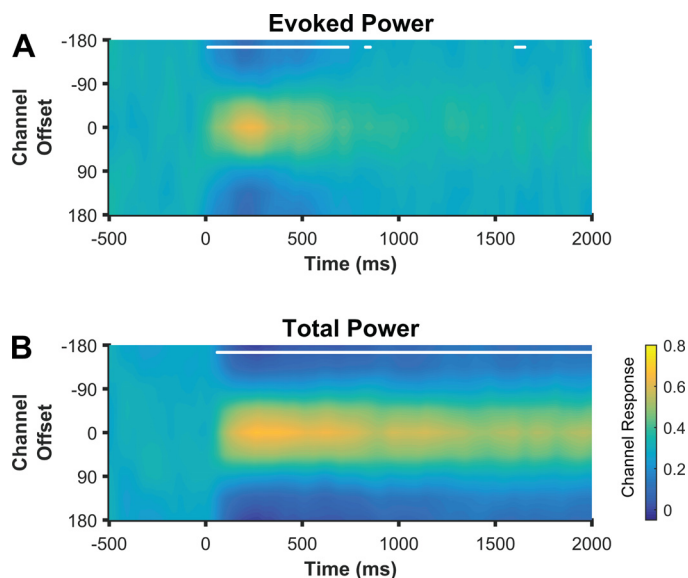


Fig. 7. Ruling out response confounds. Location CTFs reconstructed from evoked (A) and total (B) alpha (8–12 Hz) power during a spatial change detection task (*experiment 3*). Because participants could not anticipate the response (“change” vs. “no change”) during the delay period, this task eliminated any contribution of preparatory motor activity to the location CTFs. Nevertheless, total alpha power tracked location held in spatial WM throughout the delay period, whereas evoked alpha power only transiently tracked stimulus position. White markers along the top of the panels indicate the points at which CTF slope was reliably above chance as determined by a permutation test.

However, because we focused on the alpha-band, these analyses did not replicate the finding that sustained, location-selective activity is specific to the alpha band. Next, we sought to identify the frequency bands in which oscillatory power tracked stimulus location across all three experiments. To this end, we used the IEM to search time-frequency space for frequencies that carried location-specific information in *experiments 2* and *3* (as we previously reported for *experiment 1*) to obtain maps of CTF slope across time and frequency (4–50 Hz, in increments of 1 Hz) for each experiment (Fig. 8A). With these maps in hand, we then identified the points in time-frequency space that showed reliable CTF selectivity across all three experiments to create a cross-experiment map of location-selective oscillatory activity (Fig. 8B). This simple but conservative analysis revealed that evoked and total power across a range of frequency bands (~4–20 Hz) transiently tracked stimulus location, while only total alpha power tracked the remembered location throughout the delay period. The cross-experiment maps combined data from three independent experiments, with nonoverlapping groups of participants.<sup>1</sup> Therefore, this analysis provides clear evidence that location-selective oscillatory activity during WM maintenance, as reflected in the topographic distribution of oscillatory power, is specific to the alpha band.

Our results provide decisive evidence that the topography of alpha power tracks the location held in spatial WM, suggesting that alpha-band activity is related to the coding of spatial representations in WM. However, it is less clear whether other frequency bands play similar roles. Theta- and gamma-band

activity (i.e., 4–7 Hz and ~30–100 Hz, respectively) are of particular interest because they have been proposed to play a central role in coordinating cellular assemblies that code the content of WM (Lisman 2010; Roux and Uhlhaas 2014). Given that we observed no evidence of sustained location selectivity in the topographic distribution of theta or gamma power, it is tempting to conclude that the frequency bands do not contribute to the coding of spatial representations in WM. However, it is possible that these frequency bands contribute to the coding of spatial WM representations in ways that do not result in location-specific patterns of EEG power across the scalp. For example, location-specific patterns of theta-band activity may exist in hippocampal local field potentials (e.g., Agarwal et al. 2014). Such location selectivity might not necessarily produce location-specific patterns of theta power on the scalp. Thus our results do not rule out potential roles for oscillatory activity outside the alpha band in coding the content of spatial WM.

## DISCUSSION

Previous work has demonstrated that alpha power is reduced contralateral to locations held in spatial WM (Medendorp et al. 2007; Van Der Werf et al. 2008; van Dijk et al. 2010). However, those studies left it unanswered whether the topographic distribution of alpha activity tracked the precise location held in WM, or whether alpha activity reflected a lateralized memory process (e.g., a contralateral control signal) that is insensitive to the specific location that is stored. Here, we provide clear evidence that the topographic pattern of total alpha-band power precisely tracks the angular location maintained in WM. We used an inverted encoding model (IEM) to reconstruct CTFs from the pattern of EEG power across the scalp, which provided an assay of location-selective activity across the neuronal populations reflected in EEG activity. A clear pattern of results emerged over three independent experiments: while evoked and total power across a range of frequency bands transiently tracked the location of the sample stimulus, only total alpha power tracked the remembered location throughout the delay period. Furthermore, these location-specific patterns of alpha power showed the hallmark graded profile of a sensory population code. This result clearly demonstrates that alpha activity coordinates location-tuned neuronal populations rather than populations that code for more abstract variables, such as top-down control signals or categorical representations of location. Together, these results demonstrate that alpha activity is related to the sensory coding of spatial representations in WM.

Our findings build on a foundation of human neuroimaging work demonstrating that the feature content of visual WM can be recovered from voxelwise patterns of activity (e.g., Christophel et al. 2012; Emrich et al. 2013; Ester et al. 2009, 2013, 2015; Harrison and Tong 2009; Serences et al. 2009; Rigall and Postle 2012; Sprague et al. 2014). While stimulus-specific activity measured with functional magnetic resonance imaging (fMRI) allows for reconstruction of feature-selective CTFs (e.g., Ester et al. 2013, 2015), the temporal precision of this approach is limited by the sluggish hemodynamic response. In a recent study, Garcia and colleagues reconstructed time-resolved CTFs from the topographic distribution of power evoked by a flickering stimulus, highlighting the potential of

<sup>1</sup> One participant took part in both *experiments 1* and *3*. This subject was excluded from the *experiment 3* dataset for the purpose of the cross-experiment map to ensure that the data from each experiment were independent.

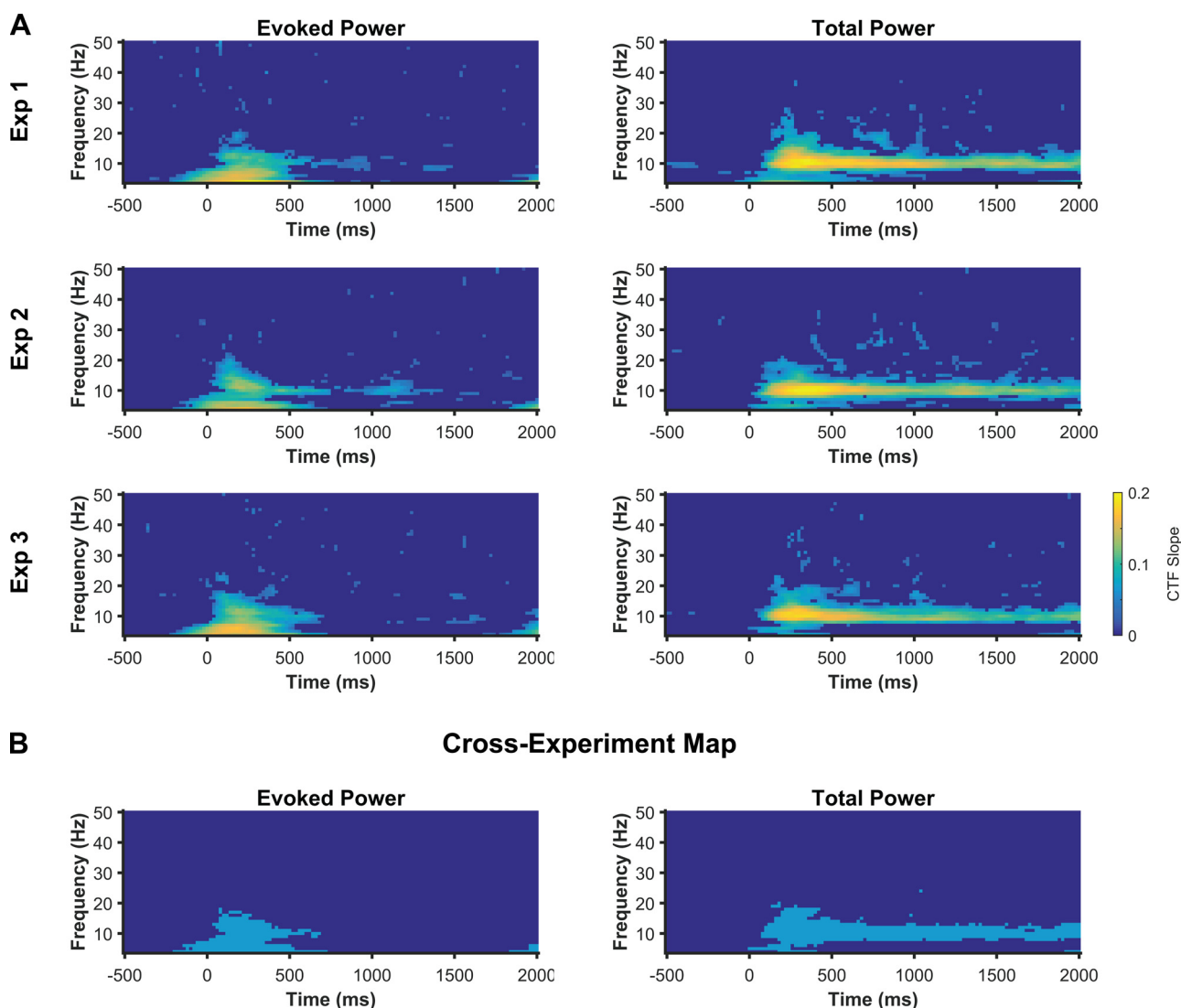


Fig. 8. Location-selective activity is specific to the alpha band. *A*: slope of CTFs reconstructed from the topographic distribution of evoked and total power across a broad range of frequencies (4–50 Hz, in increments of 1 Hz) and time for *experiments 1–3*. Points at which CTF slope was not reliably above zero as determined by a permutation test are set to zero (dark blue). *B*: cross-experiment map of the points for which CTF slope was reliably above chance for all three experiments. Reliable points are shown in light blue. Across three experiments, evoked and total power transiently tracked stimulus location after stimulus onset across a broad range of frequencies (4 to ~20 Hz) while only total alpha power tracked the content of spatial WM throughout the delay period.

combining IEMs with EEG recordings to obtain temporally-resolved stimulus-specific activity (Garcia et al. 2013). Here, we find that total alpha power tracks the content of spatial WM throughout a delay period, in the absence of rhythmic visual stimulation. Thus the intrinsic role that alpha-band activity plays in spatial WM storage enables moment-by-moment tracking of location-specific activity, without the need for a flickering stimulus. Given that the topography of alpha power covaries with attended locations (Bahramisharif et al. 2010, 2011; Rihs et al. 2007; van Gerven and Jensen 2009), we expect that this approach should also provide a powerful tool for tracking the dynamics of covert attention.

The IEM approach allowed us to reconstruct CTFs, providing an assay of location-specific activity across large populations of neurons (Serences and Saproo 2012). While single neurons are the building block for sensory codes, it is the joint activity of a population of cells that guide behavior (Butts and Goldman 2006; Jazayeri and Movshon 2006). Thus popula-

tion-level encoding models provide a good approach for linking brain and behavior (Sprague et al. 2015). This approach has already enjoyed some success. For example, Sprague and colleagues (Sprague et al. 2014) used a spatial encoding model to obtain population-level reconstructions of stimulus location from patterns of activity measured with fMRI during a spatial WM task. Sprague and colleagues found that amplitude of spatial reconstructions tracked the decline in mnemonic precision that is seen with increasing set size in a WM task. The location-specific patterns of alpha power we report here provide a new window onto population-level coding. Although we do not demonstrate it here, we expect that the topography of alpha activity should also track changes in the quality of population codes and predict behavior. Furthermore, because of the temporal resolution that EEG affords, this approach may be sensitive to rapid changes in the quality of population codes. Further work is necessary to test these predictions.

What are the cortical origins of the topographic pattern of alpha power that track the content of spatial WM? In studies of spatial attention, changes in topographic patterns of alpha power are thought to reflect synchronization of posterior visual areas tuned for unattended locations, reflecting suppression of processing in these regions (Kelly et al. 2006; Rihs et al. 2007; Thut et al. 2006). While it is tempting to conclude that the location-specific modulations of alpha activity reflect synchronization within visual cortex, it is difficult to infer the cortical source of oscillations based on EEG recordings alone. Neuroimaging studies have revealed location-specific activity in frontal, parietal, and occipital cortex during spatial attention and WM tasks (Silver and Kastner 2009; Sprague and Serences 2013; Sprague et al. 2014). Thus it is possible that location-specific patterns of alpha power might reflect synchronization within or between any of these location-selective regions.

We found that alpha activity tracked stimulus location not only during the delay period, but also while the stimulus remained in view throughout an extended encoding period (*experiment 2*). Traditionally, visual WM has been characterized as a system for the maintenance of visual inputs that are no longer present. However, recent work has challenged this view, instead suggesting that WM also constrains representation of externally available stimuli (Chun 2011; Tsubomi et al. 2013). For example, Tsubomi and colleagues demonstrated that memory load-dependent contralateral delay activity (CDA), an electrophysiological marker of maintenance in visual WM, showed a similar profile across both stimulus-absent and stimulus-present periods under the same task demands (Tsubomi et al. 2013). Here, we show that the alpha-band activity, like the CDA, plays a role in maintaining active spatial representations in both the presence and absence of visual input.

Our finding that the topography of alpha power tracks the content of spatial WM is consistent with the broad hypothesis that neuronal oscillations synchronize the cellular assemblies that code for mental representations (Fell and Axmacher 2011; Hebb 1949; Nicolelis et al. 1997; Sejnowski and Paulsen 2006; Singer and Gray 1995; Singer 1999; Watrous et al. 2015). Applied to WM, this view predicts that patterns of oscillatory activity should not only track spatial representations held in WM, but also nonspatial representations (e.g., color and orientation). Indeed, Salazar and colleagues found content-specific synchronization between frontal and parietal local field potentials in monkeys, peaking at 15 Hz. Frontoparietal synchronization tracked both the location and identity (i.e., shape) of a remembered stimulus in a delayed-match to sample task, suggesting that both identity and location are encoded in patterns of synchronization (Salazar et al. 2012). However, evidence for the role of oscillations in coordinating the code of nonspatial features is sparse, and further work is needed to examine whether neuronal synchrony plays a general role in coordinating feature-selective cellular assemblies that code the content of WM.

### Conclusions

Using an inverted spatial encoding model, we demonstrated that the topographic distribution of alpha power tracks spatial representations held in WM. These findings show that alpha-band activity plays a role in coding for spatial information held

in WM, and this approach provides a time-resolved tool for tracking the content of spatial WM.

### ACKNOWLEDGMENTS

We thank J. Evans, R. Matullo, and C. Nawawi for assistance with data collection, and T. Sprague for useful comments on the manuscript.

### GRANTS

This work was supported by National Institute of Mental Health Grant 2R01-MH-087214-06A1 to E. Awh and E. K. Vogel.

### DISCLOSURES

No conflicts of interest, financial or otherwise, are declared by the author(s).

### AUTHOR CONTRIBUTIONS

Author contributions: J.J.F., D.W.S., J.T.S., E.K.V., and E.A. conception and design of research; J.J.F. and D.W.S. performed experiments; J.J.F., D.W.S., and E.A. analyzed data; J.J.F., D.W.S., J.T.S., E.K.V., and E.A. interpreted results of experiments; J.J.F. prepared figures; J.J.F. and E.A. drafted manuscript; J.J.F., D.W.S., J.T.S., E.K.V., and E.A. edited and revised manuscript; J.J.F., D.W.S., J.T.S., E.K.V., and E.A. approved final version of manuscript.

### REFERENCES

- Agarwal G, Stevenson IH, Berényi A, Mizuseki K, Buzsáki G, Sommer FT. Spatially distributed local fields in the hippocampus encode rat position. *Science* 344: 626–630, 2014.
- Awh E, Jonides J. Overlapping mechanisms of attention and spatial working memory. *Trends Cogn Sci* 5: 119–126, 2001.
- Awh E, Vogel EK, Oh SH. Interactions between attention and working memory. *Neuroscience* 139: 201–208, 2006.
- Bahramisharif A, Heskes T, Jensen O, van Gerven MAJ. Lateralized responses during covert attention are modulated by target eccentricity. *Neurosci Lett* 491: 35–39, 2011.
- Bahramisharif A, van Gerven M, Heskes T, Jensen O. Covert attention allows for continuous control of brain-computer interfaces. *Eur J Neurosci* 31: 1501–1508, 2010.
- Brainard DH. The psychophysics toolbox. *Spat Vis* 10: 433–436, 1997.
- Brouwer GJ, Heeger DJ. Cross-orientation suppression in human visual cortex. *J Neurophysiol* 106: 2108–2119, 2011.
- Brouwer GJ, Heeger DJ. Decoding and reconstructing color from responses in human visual cortex. *J Neurosci* 29: 13992–14003, 2009.
- Butts DA, Goldman MS. Tuning curves, neuronal variability, and sensory coding. *PLOS Biol* 4: e92, 2006.
- Canolty RT, Knight RT. The functional role of cross-frequency coupling. *Trends Cogn Sci* 14: 506–515, 2010.
- Christophel TB, Hebart MN, Haynes JD. Decoding the contents of visual short-term memory from human visual and parietal cortex. *J Neurosci* 32: 12983–12989, 2012.
- Chun MM. Visual working memory as visual attention sustained internally over time. *Neuropsychologia* 49: 1407–1409, 2011.
- Delorme A, Makeig S. EEGLAB: an open source toolbox for analysis of single-trial EEG dynamics including independent component analysis. *J Neurosci Meth* 134: 9–21, 2004.
- Emrich SM, Riggall AC, LaRocque JJ, Postle BR. Distributed patterns of activity in sensory cortex reflect precision of multiple items maintained in visual short-term memory. *J Neurosci* 33: 6516–6523, 2013.
- Ester EF, Anderson DE, Serences JT, Awh E. A neural measure of precision in visual working memory. *J Cogn Neurosci* 25: 754–761, 2013.
- Ester EF, Serences JT, Awh E. Spatially global representations in human primary visual cortex during working memory maintenance. *J Neurosci* 29: 15258–15265, 2009.
- Ester EF, Sprague TC, Serences JT. Parietal and frontal cortex encode stimulus-specific mnemonic representations during visual working memory. *Neuron* 87: 893–903, 2015.
- Fell J, Axmacher N. The role of phase synchronization in memory processes. *Nat Rev Neurosci* 12: 105–118, 2011.

- Fries P.** A mechanism for cognitive dynamics: neuronal communication through neuronal coherence. *Trends Cogn Sci* 9: 474–480, 2005.
- Garcia JO, Srinivasan R, Serences JT.** Near-real-time feature-selective modulations in human cortex. *Curr Biol* 23: 515–522, 2013.
- Gazzaley A, Nobre AC.** Top-down modulation: bridging selective attention and working memory. *Trends Cogn Sci* 16: 129–135, 2012.
- Gould IC, Rushworth MF, Nobre AC.** Indexing the graded allocation of visuospatial attention using anticipatory alpha oscillations. *J Neurophysiol* 105: 1318–1326, 2011.
- Gruber WR, Klimesch W, Sauseng P, Doppelmayr M.** Alpha phase synchronization predicts P1 and N1 latency and amplitude size. *Cereb Cortex* 15: 371–377, 2005.
- Hanslmayr S, Klimesch W, Sauseng P, Gruber W, Doppelmayr M, Freunberger Pecherstorfer T, Birbaumer N.** Alpha phase reset contributes to the generation of ERPs. *Cereb Cortex* 17: 1–8, 2007.
- Harrison SA, Tong F.** Decoding reveals the contents of visual working memory in early visual areas. *Nature* 458: 632–635, 2009.
- Hebb DO.** *The Organization of Behavior*. New York: Wiley, 1949.
- Jazayeri M, Movshon JA.** Optimal representation of sensory information by neural populations. *Nat Neurosci* 9: 690–696, 2006.
- Kelly SP, Lalor EC, Reilly RB, Foxe JJ.** Increases in alpha oscillatory power reflect an active retinotopic mechanism for distractor suppression during sustained visuospatial attention. *J Neurophysiol* 95: 3844–3851, 2006.
- Klimesch W.** Alpha-band oscillations, attention, and controlled access to stored information. *Trends Cogn Sci* 16: 606–617, 2012.
- Lins OG, Picton TW, Berg P, Scherg M.** Ocular artifacts in EEG and event-related potentials I: scalp topography. *Brain Topogr* 6: 51–63, 1993a.
- Lins OG, Picton TW, Berg P, Scherg M.** Ocular artifacts in recording EEGs and event-related potentials II: source dipoles and source components. *Brain Topogr* 6: 65–78, 1993b.
- Lisman J.** Working memory: the importance of theta and gamma oscillations. *Curr Biol* 20: R490–R492, 2010.
- Medendorp WP, Kramer GFI, Jensen O, Oostenveld R, Schoffelen JM, Fries P.** Oscillatory activity in human parietal and occipital cortex shows hemispheric lateralization and memory effects in a delayed double-step saccade task. *Cereb Cortex* 17: 2364–2374, 2007.
- Nicolelis MAL, Fanselow EE, Ghazanfar AA.** Hebb's dream: the resurgence of cellular assemblies. *Neuron* 19: 219–221, 1997.
- Pelli DG.** The VideoToolbox software for visual psychophysics. Transforming numbers into movies. *Spat Vis* 10: 437–442, 1997.
- Pouget A, Dayan P, Zemel R.** Information processing with population codes. *Nat Rev Neurosci* 1: 125–132, 2000.
- Riggall AC, Postle BR.** The relationship between working memory storage and elevated activity as measured with functional magnetic resonance imaging. *J Neurosci* 32: 12990–12998, 2012.
- Rihs TA, Christoph MM, Thut G.** Mechanisms of selective inhibition in visual spatial attention are indexed by alpha-band EEG synchronization. *Eur J Neurosci* 25: 603–610, 2007.
- Roux F, Uhlhaas PJ.** Working memory and neural oscillations: alpha-gamma versus theta-gamma codes for distinct WM information? *Trends Cogn Sci* 18: 16–25, 2014.
- Salazar RF, Dotson NM, Bressler SL, Gray CM.** Content-specific frontoparietal synchronization during visual working memory. *Science* 338: 1097–1101, 2012.
- Saproo S, Serences JT.** Attention improves transfer of motion information between V1 and MT. *J Neurosci* 34: 3586–3596, 2014.
- Sejnowski TJ, Paulsen O.** Network oscillations: emerging computational principles. *J Neurosci* 23: 1673–1676, 2006.
- Serences JT, Ester EF, Vogel EK, Awh E.** Stimulus-specific delay activity in human primary visual cortex. *Psychol Sci* 20: 207–214, 2009.
- Serences JT, Saproo S.** Computational advances towards linking BOLD and behavior. *Neuropsychologia* 50: 435–446, 2012.
- Silver MA, Kastner S.** Topographic maps in human frontal parietal cortex. *Trends Cogn Sci* 13: 488–495, 2009.
- Singer W.** Neuronal synchrony: a versatile code for the definition of relations? *Neuron* 24: 49–65, 1999.
- Singer W, Gray CM.** Visual feature integration and the temporal correlation hypothesis. *Annu Rev Neurosci* 18: 555–586, 1995.
- Sprague TC, Ester EF, Serences JT.** Reconstructions of information in visual spatial working memory degrade with memory load. *Curr Biol* 24: 2174–2180, 2014.
- Sprague TC, Saproo S, Serences JT.** Visual attention mitigates information loss in small- and large-scale neural codes. *Trends Cogn Sci* 19: 215–226, 2015.
- Sprague TC, Serences JT.** Using human neuroimaging to examine top-down modulation of visual perception. In: *An Introduction to Model-Based Cognitive Neuroscience*, edited by Forstmann BU, Wagenmakers E-J. New York: Springer, 2015.
- Sprague TC, Serences JT.** Attention modulates spatial priority maps in the human occipital, parietal and frontal cortices. *Nat Neurosci* 16: 1879–1887, 2013.
- Suchow JW, Brady TF, Fougner D, Alvarez GA.** Modeling visual working memory with the MemToolbox. *J Vision* 13: 1–8, 2013.
- Thut G, Nietzel A, Brandt SA, Pascual-Leone A.** Alpha-band electroencephalographic activity over occipital cortex indexes visuospatial attention bias and predicts visual target detection. *J Neurosci* 26: 9494–9502, 2006.
- Tsubomi H, Fukuda K, Watanabe K, Vogel EK.** Neural limits to representing objects still within view. *J Neurosci* 33: 8257–8263, 2013.
- Van Der Werf J, Jensen O, Fries P, Medendorp P.** Gamma-band activity in human posterior parietal cortex encodes the motor goal during delayed prosaccades and antisaccades. *J Neurosci* 28: 8397–8405, 2008.
- Van Dijk H, Van Der Werf J, Mazaheri A, Medendorp P, Jensen O.** Modulations in oscillatory activity with amplitude asymmetry can produce cognitively relevant event-related responses. *Proc Natl Acad Sci USA* 107: 900–905, 2010.
- van Gerven M, Jensen O.** Attention modulations of posterior alpha as a control signal for two-dimensional brain-computer interfaces. *J Neurosci Meth* 179: 78–84, 2009.
- Watrous AJ, Fell J, Ekstrom AD, Axmacher N.** More than spikes: common oscillatory mechanisms for content specific neural representations during perception and memory. *Curr Opin Neurobiol* 31: 33–39, 2015.
- Wilken P, Ma WJ.** A detection theory account of change detection. *J Vision* 4: 1120–1135, 2004.
- Worden MS, Foxe JJ, Wang N, Simpson GV.** Anticipatory biasing of visuospatial attention indexed by retinotopically specific alpha-band electroencephalography increases over occipital cortex. *J Neurosci* 20: RC631, 2000.
- Zhang W, Luck SJ.** Discrete fixed-resolution representations in visual working memory. *Nature* 453: 233–235, 2008.